INTERNATIONAL JOURNAL OF HYDROGEN ENERGY 39 (2014) 21335–21342

Available online at www.sciencedirect.com

ScienceDirect

journal homepage: www.elsevier.com/locate/he

The effect of a perforated plate on the propagation of laminar hydrogen flames in a channel – A numerical study

C.J. Wang [a], J.X. Wen [b,*]

[a] State Key Laboratory of Fire Science, University of Science and Technology of China, Hefei, 230027, Anhui, China
[b] Warwick FIRE, School of Engineering, University of Warwick, Coventry, CV4 7AL, UK

ARTICLE INFO

Article history:
Received 22 December 2013
Received in revised form
30 September 2014
Accepted 20 October 2014
Available online 7 November 2014

Keywords:
Laminar flame
Porous media model
Flame acceleration
Flame quenching

ABSTRACT

Laminar hydrogen flame propagation in a channel with a perforated plate is investigated using 2D reactive Navies-Stokes simulations. The effect of the perforated plate on flame propagation is treated with a porous media model. A one step chemistry model is used for the combustion of the stoichiometric H_2–air mixture. Numerical simulations show that the perforated plate has considerable effect on the flame propagation in the region downstream from the perforated plate and marginal effect on the upstream region. It is found to squeeze the flame front and result in a ring of unburned gas pocket around the flame neck. The resulting abrupt change in flow directions leads to the formation of some vortices. Downstream of the perforated plate, a wrinkled "M"-shape flame is observed with "W" shape flame speed evolution, which lastly turns back to a convex curved flame front. Parametric studies have also been carried out on the inertial resistance factor, porosity, perforated plate length and its location to investigate their effects on flame evolution. Overall, for parameter range studied, the perforated plate has an effect of reducing the flame speed downstream of it.

Introduction

Hydrogen is a clean substitute for fossil fuels and seen as a potential energy carrier for the future. However, hydrogen has a wide flammability range from 4% to 75% and high reactivity with a laminar flame speed around 6 times that of typical hydrocarbon fuels. The commercial exploitation of hydrogen will inevitably involve its transportation through pipelines from the point of production or delivery to the point of demand. While the research has been ongoing elsewhere on the related issues of hydrogen embrittlement and adding hydrogen to the existing natural gas pipeline network, the present study is conducted in the context of using porous plate type of flame arresters to enhance safety during pipeline transmission and in process equipment.

Accidental ignition of fuel in pipelines can lead to explosions and in some cases transition from deflagration-to-detonation (DDT). As such, flame arrestors are frequently used in industry to enhance safety. A common type arrester is based on the quenching effect of the porous material, which depends on the pore characteristic dimensions and the flame

* Corresponding author.
E-mail address: Jennifer.Wen@warwick.ac.uk (J.X. Wen).
http://dx.doi.org/10.1016/j.ijhydene.2014.10.081

properties (i.e., the flame thickness and laminar burning velocity) [1,2]. Insight of the quenching mechanism will be of assistance towards increasing the effectiveness of such arresters.

Among the literature, some experimental work has been carried out on flame interaction with porous media. Khanna et al. [2] studied methane combustion in a porous medium burner with porosity of 0.87 upstream and 0.84 downstream. Ellzey and Goel [3] measured carbon monoxide and nitric oxide emissions of fuel/air mixture using a two stage porous media burner. Tseng and Howell [4] studied combustion of liquid fuels in a porous radiant burner. These studies focused on burner flames. For propagating flames, Babkin et al. [5], Pinaev [6] and Makris et al. [7] investigated steady flame and detonation propagation in vertical tubes filled with sand and spherical beads. Flame propagation in porous media at speed greater than 5 m/s was found to produce a local pressure rise ahead of the flame. Johansen et al. [8–10] investigated flame propagation in a horizontal channel filled with spherical beads and found that flame propagating above the bead layer had a higher speed than the speed of sound in the combustion products [9]. Ciccarelli et al. [10] found that flame of a stoichiometric hydrogen-air mixture accelerated rapidly in a 7.62 cm square cross-section channel filled with 1.27 cm diameter beads.

A number of numerical investigations on flame interaction with porous media have also been reported. Zhou and Pereira [11] investigated one-dimensional combustion on a porous burner using detailed reaction mechanism of methane/air. Malico et al. [12] simulated a flame in a 10 kW porous burner. Zhao et al. [13] numerically studied the CH_4/air premixed gas combustion in a porous media burner using detailed chemistry. Zheng et al. [14] performed numerical studies on flame inclination in porous media combustors.

However, none of these were conducted in the context of the flame arresting potential of the porous materials. Overall, relatively little study has been carried out about flame interaction with porous media, especially for low speed flame propagation in a channel obstructed with perforated plate. Depending on the pore characteristic dimensions and the flame characteristics, the porous material might have a quenching effect rather than accelerating the flame as in the case investigated by Ciccarelli et al. [10]. In the present, we aim to gain insight of the flame and porous plate interaction in a channel through numerical study, focussing on the effect of the porous plate with pore characteristic dimensions on the flame structure and propagation mechanism. Such study does not directly address the potential quenching mechanism but shades light on the changing flame behaviour when going through a perforated plate. Such fundamental understanding will serve as the basis towards investigating the quenching mechanism of perforated plates.

Numerical modelling

Governing equations and numerical schemes

The following assumptions are made in order to represent the perforated plate as porous media:

(1) The perforated plate is non-catalytic and homogeneous.
(2) Radiation heat transfer from the wall, gas and the perforated plate are also neglected.
(3) The porosity variation near the tube wall is not considered.

Based on the above assumption, the governing equations can be described as follows:

Mass conservation equation:

$$\frac{\partial \rho}{\partial t} + \nabla \cdot (\rho \vec{U}) = 0 \tag{1}$$

Momentum conservation equation:

$$\frac{\partial \psi \rho \vec{U}}{\partial t} + \nabla \cdot (\rho \vec{U}\vec{U}) = -\nabla p + \nabla \cdot \vec{\tau} + S_d \tag{2}$$

Energy conservation equation:

$$\frac{\partial \left(\psi \rho h_s + (1-\psi)\rho_p h_{s,p}\right)}{\partial t} + \nabla \cdot (\rho \vec{U} h_s) = \frac{dp}{dt} + \vec{\tau} : \nabla \vec{U} + \nabla \cdot \left[k_{eff} \nabla T + \sum_{i=1}^{NS} \rho D h_{si} \nabla Y_i\right] + \dot{q}''' \tag{3}$$

Species conservation equation:

$$\frac{\partial \rho Y_i}{\partial t} + \nabla \cdot (\rho \vec{U} Y_i) = \nabla \cdot (\rho D \nabla Y_i) + S_i \tag{4}$$

where ρ and ρ_p are the gas and porous media densities. $\vec{U}$ is the velocity and t is time. The ratio $Y_i = \rho_i/\rho$ denotes the i-th species mass fraction. NS is the total number of species. p, T and h_s denote pressure, temperature and sensible enthalpy, respectively. h_{si} is the sensible enthalpy *of the* i-th specie. $k_{eff} = \psi k_g + (1-\psi)k_p$ where k_g is gas thermal conductivity and k_p is porous media thermal conductivity. $\rho D = \mu = \frac{k_g}{C_p} = z_0\, T^{0.7}$ [15,16], where D, μ, C_p and z_0 are the diffusion coefficient, viscosity coefficient, specific heat capacity at constant pressure and transport constant, respectively. $\vec{\tau} = \mu\left[\left(\nabla \vec{U}\right) + (\nabla \vec{U})^T - \frac{2}{3}(\nabla \cdot \vec{U})I\right]$, where I is unit vector. $h_{s,p}$ denotes the sensible enthalpy of porous media. ψ is the porosity of the perforated plate. S_d is composed of two parts, a viscous loss term and an inertial loss term due to the perforated plate and can be expressed as

$$S_d = -\left(\mu D + \frac{1}{2}\rho \left|\vec{U}\right| F\right)\vec{U} \tag{5}$$

where F is the inertial resistance factor, and can be viewed as a loss coefficient per unit length along the flow direction due to the effect of porous media.

Based on the mass interaction law, the mass production/sink rate of the i-th species due to gas reaction can be derived as:

$$S_i = \nu_i W_i \dot{\omega} \tag{6}$$

where ν_i and W_i denotes the stoichiometric coefficient and molar weight of the i-th species. $\dot{\omega}$ denotes the molar production rate of product per unit volume.

The heat release rate per unit volume from a chemical reaction $\dot{q}'''$ can be expressed as

$$\dot{q}''' = \dot{\omega} q \tag{7}$$

where q is chemical heat release per unit volume.

Equations (1)–(4) can be written in the form of a general transport equation, given below and used to present the Finite Volume discretisation in OpenFOAM framework [17,18].

$$\int_V \frac{\partial \rho\phi}{\partial t} dV + \int_V \nabla\cdot(\rho U\phi) dV - \int_V \nabla\cdot(\rho\Gamma_\phi \nabla\phi) dV = \int_V S_\phi(\phi) dV \tag{8}$$

where ϕ, V, Γ_ϕ denote general scalar property, volume of the cell and diffusivity, respectively.

Before the actual Finite Volume discretisation, the source term $S_\phi(\phi)$ needs to be linearised:

$$S_\phi(\phi) = S_u + S_t\phi \tag{9}$$

where constant part S_u and linear part S_t in the soure term can depend on ϕ.

So Equation (8) can be re-written using an implicit Euler discretization [18] as

$$\frac{(\rho_P\phi_P)^{n+1} - (\rho_P\phi_P)^n}{\Delta t} V_P + \sum_f \vec{S}_f \cdot (\rho\vec{U})_f^n (\phi_f)^{n+1} - \sum_f \left[(\rho\Gamma_\phi)_f \vec{S}_f \cdot \left(\frac{\phi_N - \phi_P}{|\vec{d}|} \right)_f \right]^n = (S_u V_P)^n + S_t V_P (\phi_P)^{n+1} \tag{10}$$

where P and N denote the cell point. Subscription f denotes cell surface. $\vec{S}$ and $\vec{d}$ are face area vector and vector between P and N, respectively. $()^{n+1}$ and $()^n$ are the values at the current step and the previous step, respectively. The surface field ϕ_f is calculated by the total variation diminishing (TVD) scheme [18].

From Equations (1)–(4), there exists some coupling effects for velocity, temperature and species transport, e.g. the temperature evaluated from the sensitive enthalpy in the energy conservation equation, will be determined by velocity from the momentum equation and density from the mass conservation equation, etc. Temperature change decides the pressure while species concentration affects the density. Both influence the velocity value when solving the momentum equations. Hence, the Pressure-Implicit with Splitting of Operators (PISO) algorithm was employed. The computational procedure can be described as follows:

(1) Define the initial conditions for all the parameters.
(2) Start the calculation of the new time-step values.
(3) Solve the momentum predictor equation by using the available face fluxes.
(4) Iterate the PISO loop until the target tolerance for pressure and velocity is achieved. So pressure and velocity fields are obtained for the current time-step as well as the new conservative fluxes.
(5) Using these new conservative fluxes, solve all other equations.
(6) If the current time is smaller than the end time, go back to step 2.

Chemistry model

For the calculation of the chemical source terms in stoichiometric hydrogen-air combustion, the one step chemistry model developed by Wang et al. [19] is adopted. Following the similar approach used by Bane et al. [20] and Kessler et al. [16] to obtain the reaction order, reaction heat, activation energy etc, this model was developed by proposing a new method to determine the reaction order of fuel or Oxidizer, and predict transport coefficients. Based on the reaction order calculation, the hydrogen-air reaction is of second order and the power of fuel is close to 1. Therefore, the one step Arrhenius kinetics for hydrogen-air combustion can be written as

$$\dot{\omega} = A[O][F]\exp\left(-\frac{E_a}{RT}\right) \tag{11}$$

where [O] and [F] are molar concentrations of the oxidizer and fuel respectively. E_a and R represent activation energy and the universal gas constant, respectively.

The model parameters in the one step chemistry model, as determined using Wang et al.'s approach are summarized in Table 1. These values are similar to those used by Gamezo et al. [15] in their hydrogen DDT calculations but differences exist in the reaction order, the pre-exponential factor and the transport coefficients as the present model takes oxidizer concentration into account when determining the parameters for the Arrhenius kinetics.

Model validation

For model validation, the one-dimensional steady Zeldovich-von Neumann-Doering (ZND) wave and the free-propagating laminar flame were firstly simulated using both the current one step chemistry model as well as that of Gamezo et al. [15]. The predicted temperature, pressure and velocity distributions are presented in Figs. 1 and 2. As can be seen from Fig. 1, at $X = X_d = 0.01927$ mm, the predicted pressure and temperature distributions are in excellent agreement with the maximum discrepancy in the predicted pressure being less than 0.8% and temperature less than 2.4%. For the predictions of the free-propagating laminar flame shown in Fig. 2, the temperature and velocity are kept constant both upstream and downstream of the flame surface. Across it, the

Table 1 – Model parameters for stoichiometric hydrogen–air mixture.

Initial parameters	P_0	1 atm	Initial pressure
	T_0	293 k	Initial temperature
Known paramters [3]	T_b	7.289 T_0	Post-flame temperature
	S_l	298 cm/s	Laminar flame speed
	X_d	0.01927 cm	Half reaction length
	D_{CJ}	1.993×10^5 cm/s	Chapman-Jouguet (CJ) detonation velocity
Predicted parameters	A	1.13×10^{15} $cm^3/(mol\cdot s)$	Pre-exponential factor
	E_a	46.37 RT_0	Activation energy
	q	43.28 RT_0/M	Chemical heat release
	γ	1.17	Specific heat ratio
	z_0	7.0×10^{-5} $g/(cm\cdot s\cdot K^{0.7})$	Transport constant

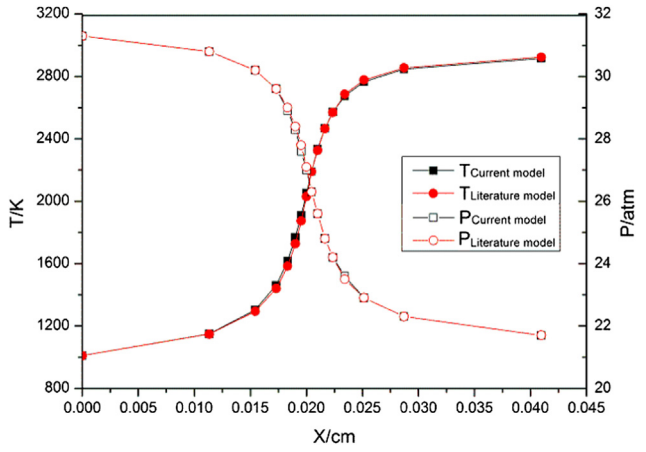

Fig. 1 – Temperature and pressure for steady ZND wave.

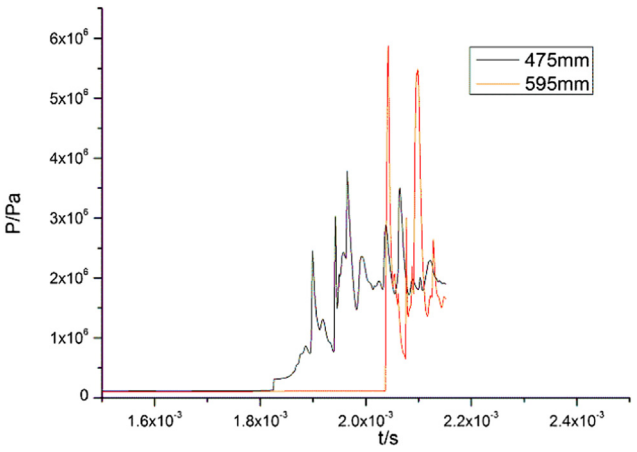

Fig. 3 – Pressure profiles at two corresponding locations in an obstructed channel (Case B [5]).

temperature and velocity are abruptly changed. The predicted temperature and velocity distributions by the two models are within 1.4% of each other. These two tests verify that the current Arrhenius model is in excellent agreement with that of Gamezo et al. [15].

To further validate the present model, we simulated flame acceleration and deflagration-to-detonation transition in an obstructed tube with the same geometric dimension and set up as case B in Teodorczyk's experiments [21]. The tube width was 20 mm. All obstacles had the same height of 10 mm. A hot burning material with radius of 0.005 mm at the centre of the left wall was defined to represent the ignition region. Extra energy in the same order of the chemistry-energy was imposed to trigger ignition. Fig. 3 presents the pressure profiles at corresponding locations. The predicted peak pressures are 3.75 MPa at 475 mm and 5.81 MPa at 595 mm from the ignition centre. Both values are within 3% of the experimental measurements.

Results and discussion

The computational domain is shown in Fig. 4. The channel is 82 cm long and 2 cm wide. It is closed at the left end and open at the right end. The perforated plate of D2 in length is mounted at a distance D1 away from the left end. This plate has the thermal conductivity $k_p = 16.27$ W/m·K. The channel is filled with stoichiometric H_2–air mixture at 1,01,325 Pa and 293 K. A half-round ignition region of 5 mm radius full of burning materials was set at the centre of the left wall.

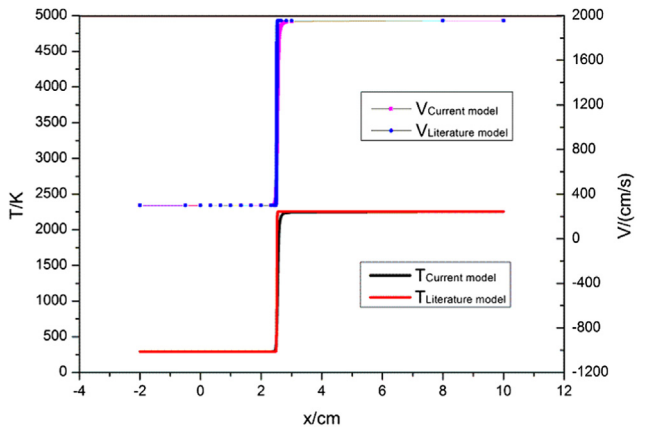

Fig. 2 – Temperature and pressure for free-propagating laminar flame.

Flame evolution with or without perforated plate

Fig. 5 presents the predicted temperature contours. Generally, the flame front divides the flow field into two parts. For current laminar flame, even though the pressure wave is continuously generated by the chemical energy release from combustion, its effect on the unreacted region ahead of the flame front is negligible. Behind the flame front, the flame temperature is kept close to constant and about 2200 K. Up to 36 ms, the temperature contours resemble closely to the predictions for an unobstructed channel as shown in Fig. 6. Due to the wall effect, the flame has a convex curved front which gradually turns sharper as it propagates. Propagating through the perforated plate, it has more profound effect to cause the centre of the flame to decelerate in comparison with edge near the wall. The curvature of the flame front gradually reduces. At 48 ms when the flame emerges after passing through the perforated plate, its front turns almost planar with the flame close to the wall catching up with the middle part of the flame. At 50 ms, the flame close to the wall exceeds the middle part, and the flame turns to a concave shape. As the edge of the flame continues to travel faster than the centre because of the influence of the perforated plate, a wrinkled

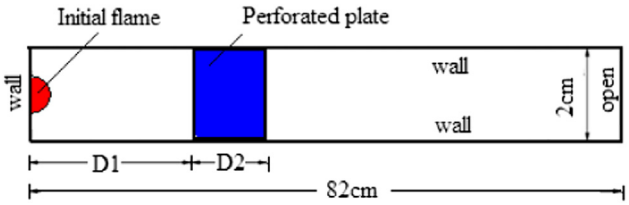

Fig. 4 – Computational domain.

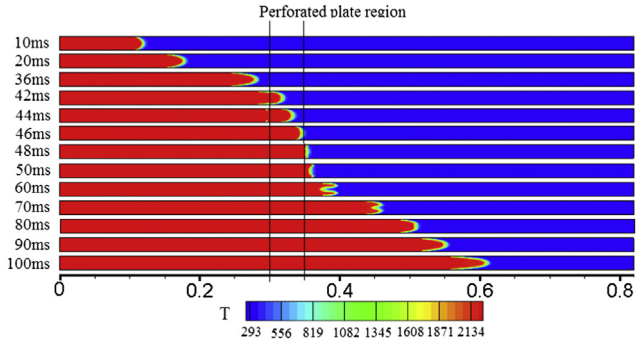

Fig. 5 – Typical flame propagation through a perforated plate (F = 80, ψ = 0.8, D1 = 0.3 m, D2 = 0.05 m).

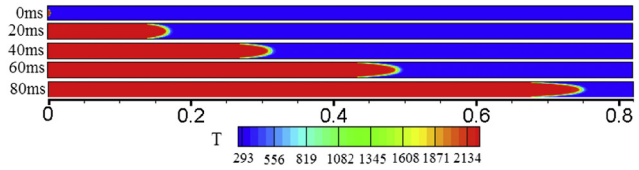

Fig. 6 – Flame propagation in an unobstructed channel.

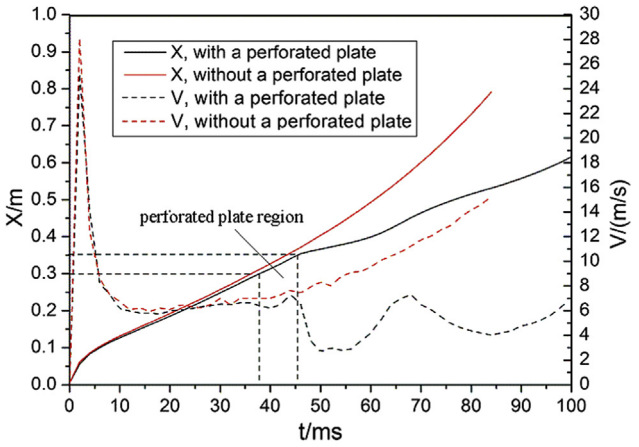

Fig. 8 – Flame front positions and speeds with or without a perforated plate.

"M" flame can be observed at 60 ms. However, this "M" flame does not last long as the flame recovers from the influence of the plate and its centre gradually catching up in speed and picking up more speed than the edge near the wall. At 80 ms, the two humps have disappeared and the flame propagates again with a convex front.

In Fig. 7, we zoom in on the temperature contours at three selected times and superimpose the streamlines as vectors on them. In Fig. 7(a) at 42 ms, the flame front is propagating through the perforated plate. Limited by the porosity, the flame head is squeezed and a flame "neck" is observed. Around this "neck", the flow direction is evidently changed. In Fig. 7(b) at 44 ms, the flame front is still in the perforated plate. Due to the aforementioned squeezing effect, the flame head continues to enlarge leaving unburned gas pocket around the flame neck. The flow direction in flame head is abruptly changed, resulting in the formation of two vortices, which can be seen more clearly in Fig. 7(d) which is a blown up image of the top vortex region in Fig. 7(b). In Fig. 7(c) at 60 ms after the flame emerges from the perforated plate, it is observed that the streamlines emit outwards from point S, which acts like a hot spot with relatively higher heat release rate, resulting in local flame acceleration.

Fig. 8 compares flame front positions and speeds with or without a perforated plate. The flame speed is averaged from that recorded in the numerical simulations every 2 ms. Following ignition, the flame front quickly accelerates to a peak value in 2 ms. Then it decelerates sharply from about 28 m/s to 6.5 m/s within the next 8 ms; and maintains this speed until entering the perforated plate. During this period, the perforated plate has minor effect on flame propagation, and the flame front position and speed closely match those without a perforated plate. Further downstream, in the case without a perforated plate, the flame gradually accelerates and reaches about 15 m/s when arriving at the open end. For

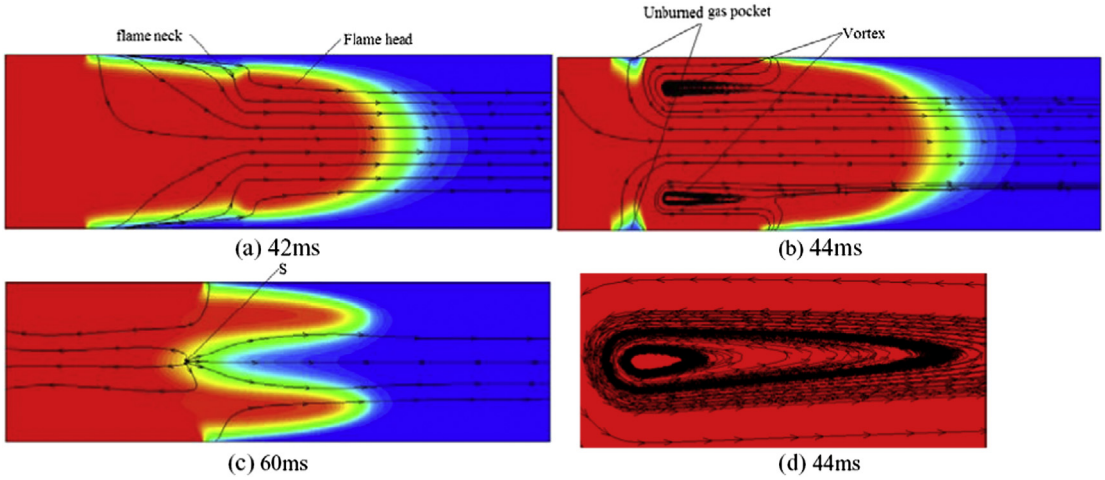

Fig. 7 – Enlarged flame images at given time.

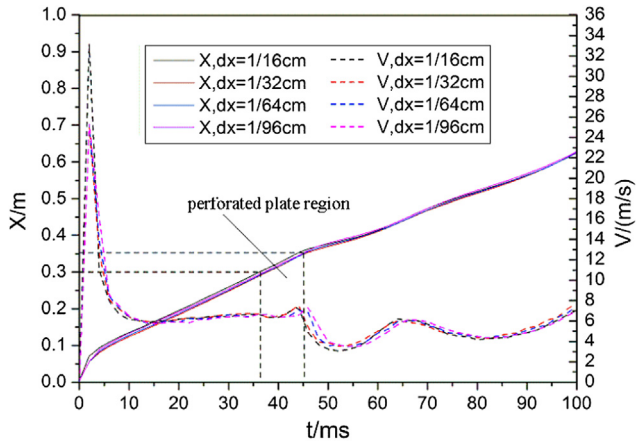

Fig. 9 – Flame front positions and speeds for four grid resolutions (F = 40, ψ = 0.8, D1 = 0.3 m, D2 = 0.05 m).

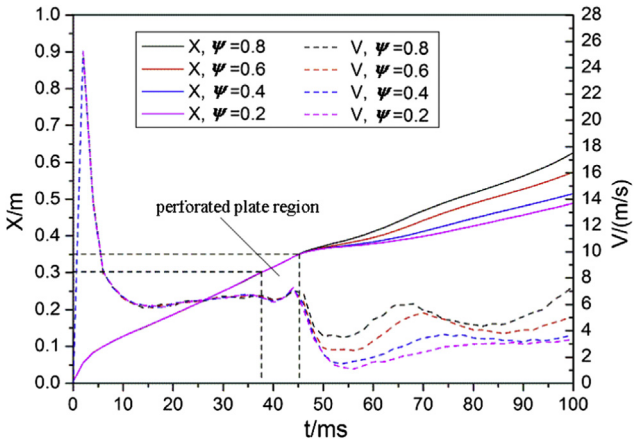

Fig. 11 – Flame front position and speed for different ψ (F = 40, D1 = 0.3 m, D2 = 0.05 m).

the case with a perforated plate, the flame decelerates first when going through the plate and then accelerates again while still going through the plate. Downstream of the perforated plate, the flame speed undergoes a change with "W" shape, i.e. it decelerates first and then re-accelerates to another peak value. Later, the flame decelerates again and then re-accelerates until the end of the simulation at 100 ms. Comparing the flame speed profile with that of the temperature contours in Fig. 5, it is found that the "W" shape in the flame speed occurs over the same period as the "M" flame front evolution. Overall, the perforated plate has an effect of reducing the flame speed emerging at the end of the channel.

Grid sensitivity study

In order to examine the effect of grid resolutions, computations were carried out with 4 different numerical resolutions dx = 1/16 cm, 1/32 cm, 1/64 cm and 1/96 cm. Fig. 9 presents the predicted flame front positions and speeds from these 4 set of predictions in which all other parameters are kept the same. It is found that the first peak value of the flame front for dx = 1/16 cm is much larger than those for dx = 1/32 cm, 1/64 cm and 1/96 cm. This implies that the ignition region is under-resolved in this case. As to the flame front trace and "W" shape of the flame speed, the 4 set of simulations produced very close predictions, indicating that apart from the coarsest resolution considered dx = 1/16 cm, the other three grid resolutions produce very similar. On this basis, the grid resolution of dx = 1/64 cm is chosen for the subsequent numerical simulations in the present study.

The effect of inertial resistance factor F

The most important characteristic parameters of a perorated plate includes its inertial resistance factor F and porosity ψ.

In order to clarify the effect of inertial resistance factor F of the perforated plate on the flame, five F values were considered, i.e. F = 10, 20, 30, 40 and 80. Fig. 10 shows the flame front position and speed for the different F, where ψ = 0.8, D1 = 0.3 m and D2 = 0.05 m are kept same. Before the flame

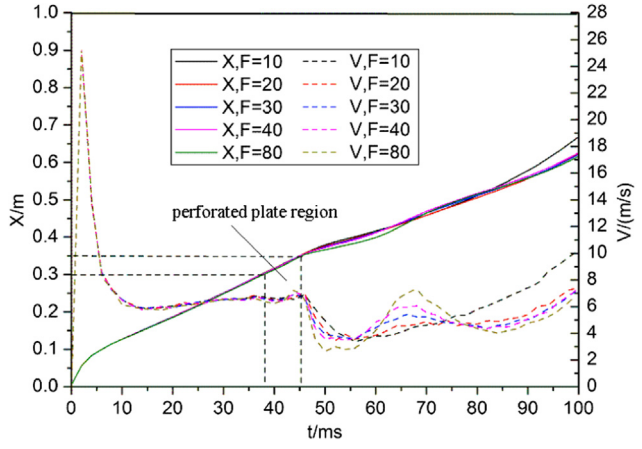

Fig. 10 – Flame front position and speed for different F (ψ = 0.8, D1 = 0.3 m, D2 = 0.05 m).

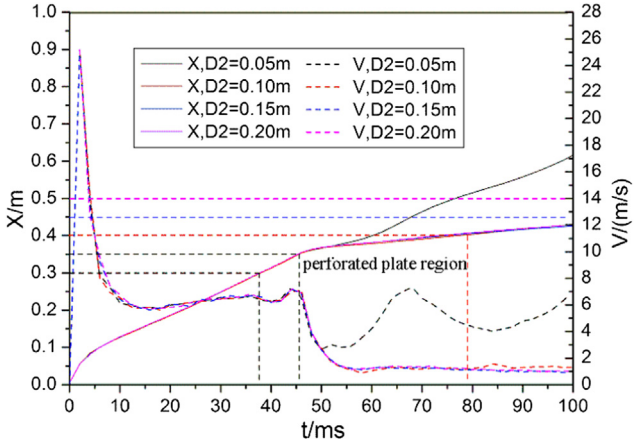

Fig. 12 – Flame front position and speed for different D2 (F = 80, ψ = 0.8, D1 = 0.3 m).

front emerges from the perforated plate, the differences in F have marginal effect on the flame front and speed predictions, implying that the inertial resistance of the perforated plate only has marginal effect on the flame propagation upstream and through it. Downstream from the perforated plate, the differences in the predictions become obvious. Firstly, the predicted flame front traces become gradually more different from each other and then closer again before repeating this changing pattern. Secondly, for the case with F = 10, the flame speed firstly decreases and then increases while for the other cases, the flame speed undergoes a change of "W" shape and the gradient of flame speed rises with increasing value of F.

Effect of porosity ψ

Four different ψ values are investigated, i.e. 0.8, 0.6, 0.4 and 0.2 while the other parameters are kept same. As shown in Fig. 11 and similar to the cases of F, before the flame emerges from the perforated plate, the effect of ψ on the predicted flame front traces and flame speeds are marginal. Downstream of the perforated plate, the predicted flame front traces start to deviate from each other. The larger the ψ value, the faster the flame propagates because the gas flow is less obstructed.

Effects of thickness D2 and mount location D1

Further parametric studies are conducted on the two geometric parameters D2 and D1. Fig. 12 presents flame front position and speed for different D2, where F = 80, ψ = 0.8 and D1 = 0.3 m. In Fig. 12, the region between the two black 90-degree dashed connecting lines is the perforated plate region for D2 = 0.05 m; the region between the first black 90-degree dashed connection line and the red one is for D2 = 0.10 m. For the other two cases, as the flame has not emerged from the perforated plate at the end of the 100 ms simulations, only a blue horizontal line and a magenta one are seen. The start line of the perforated plate region for D2 = 0.15 m or D2 = 0.2 m is the same as that for the other two. Again the differences only exist downstream of the perforated plate. For D2 = 0.05 m, flame front trace is evidently separated from the other three, and the flame speed change exhibits a "W" shape. For the other cases, the flame front trace and speed have little difference. Only very slight increase is observed for D2 = 0.10 m when the flame front propagates out of the perforated plate. The flame front is firstly decelerated and then keeps almost constant propagation speed.

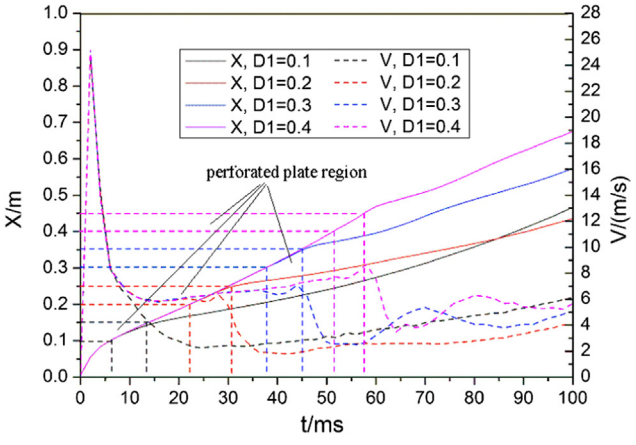

Fig. 13 – Flame front position and speed for different D1 (F = 40, ψ = 0.6, D2 = 0.05 m).

Fig. 13 presents the flame front position and speed for different D1, where F = 40, ψ = 0.6 and D2 = 0.05 m. The region between the two 90-degree dashed connecting lines with the same colour corresponds to the perforated plate region for the case with correspondingly the same colour. It is found that the perforated plate for D1 = 0.1 does not cause the flame speed to behave in "W" shape. The flame propagation in this case is similar to the case without a perforated plate. The only difference is that a very small flame speed increase can be seen downstream of the perforated plate. With increasing D1, the start position of "W" shape of flame speed moves towards the downstream direction, flame speed at left leg of "W" drops more steeply, and "W" shape turns more evident.

Conclusions

A series of numerical simulations have been carried out on the effect of a perforated plate on laminar hydrogen flame propagation in a channel. In the upstream region of the perforated plate, the predicted flame front behaves almost the same as that in the channel without a perforated plate. The flame propagates with a convex curved front which gradually turns sharper. Through the perforated plate, the flame front is squeezed and leaves behind unburned gas pocket around its neck. The abrupt change in flow directions also result in two vortices. Downstream from the perforated plate, a wrinkled "M"-shape flame is observed, which gradually turns back to a convex curved flame front. In this process, a source is observed which emits streamlines outwards and it is possibly like a hot spot with high heat release for accelerating the flame propagation.

Parametric studies have also been carried out on the effects of the inertial resistance factor, porosity, perforated plate length and its location on flame evolution. In most cases, the "W" shaped flame speed curves are predicted downstream from the perforated plate. This is distinctively different from flame propagation in channels without a perforated plate. The occurrence of this "W" shape curve is observed to correspond to the "M"-shape flame evolution. It was also found that all these parameters only have marginal effect on the flame propagation upstream of the perforated plate. In the downstream region, these parameters evidently change the shapes of the "W" flame speed curves. With decreasing porosity, or increasing inertial resistance factor and perforated plate distance from the left end, the flame front speed decrease faster at the left leg of the "W". The decrease of the porosity has the effect of reducing the curvature of the "W". On the contrary, the increase in inertial resistance factor and perforated plate distance leads to increase in the curvature. Overall, for parameter range studied, the perforated plate has an effect of reducing the flame speed emerging at the end of the channel. These findings will be of

assistance to further study about the quenching mechanism of porous plate type of flame arresters.

Acknowledgements

This project was supported by EU FP7 IIF-FP7 project (Grant No. 909658) and the National Natural Science Foundation of China (Grant No. 51376174).

REFERENCES

[1] Hsu PF, Evans WD, Howell JR. Experimental and numerical study of premixed combustion within non-homogeneous porous ceramics. Combust Sci Technol 1993;90:149–72.
[2] Khanna V, Goel R, Ellzey JL. Measurements of emissions and radiation for methane combustion within a porous medium burner. Combust Sci Technol 1994;99:133–42.
[3] Ellzey JL, Goel R. Emissions of CO and NO from a two stage porous media burner. Combust Sci Technol 1995;107:81–91.
[4] Tseng CJ, Howell JR. Combustion of liquid fuels in a porous radiant burner. Combust Sci Technol 1996;112:141–61.
[5] Babkin VS, Korzhavin AA, Bunev VA. Propagation of premixed gaseous explosion flames in porous media. Combust Flame 1991;87:182–90.
[6] Pinaev AV. Combustion modes and flame propagation criteria for an encumbered space. Comb Expl Shock Waves 1994;30(4):454–61.
[7] Makris A, Oh TJ, Lee JHS, Knystautas R. Critical diameter for the transmission of a detonation wave into a porous medium. Proc Combust Inst 1994;25:65–71.
[8] Johansen C, Ciccarelli G. Combustion in a horizontal channel partially filled with porous media. Shock Waves 2008;18:97–106.
[9] Ciccarelli G, Hlouschko S, Johansen C, Karnesky J, Shepherd JE. The study of geometric effects on the explosion front propagation in a horizontal channel with a layer of spherical beads. Proc Combust Inst 2009;32:2299–306.
[10] Ciccarelli G, Johansen C, Parravani M. Transition in the propagation mechanism during flame acceleration in porous media. Proc Combust Inst 2011;33:2273–8.
[11] Zhou XY, Pereira JCF. Numerical study of combustion and pollutants formation in inert nonhomogeneous porous media. Combust Sci Technol 1997;130:335–64.
[12] Malico I, Zhou XY, Pereira JCF. Two-dimensional numerical study of combustion and pollutants formation in porous burners. Combust Sci Technol 2000;152:57–79.
[13] Zhao P, Ye T, Jiang H, Chen Y. Study of the mechanisms of the flame propagation and stabilization in porous media. Sci China Ser E Tech Sci 2008;51:871–81.
[14] Zheng CH, Cheng LM, Saveliev A, Luo ZY, Cen KF. Numerical studies on flame inclination in porous media combustors. Int J Heat Mass Transfer 2011;54:3642–9.
[15] Gamezo VN, Ogawa T, Oran ES. Numerical simulations of flame propagation and DDT in obstaucted channels filled with hydrogen-air mixture. Proc Combust Inst 2007;31:2463–71.
[16] Kessler DA, Gamezo VN, Oran ES. Simulations of flame acceleration and deflagration and deflagration-to-detonation transitions in methane-air systems. Combust Flame 2010;157:2063–77.
[17] Jasak H. Error analysis and estimation for the finite volume method with applications to fluid flows. London: Imperial College; 1996 (PhD thesis).
[18] OpenFOAM programmer's guide (version 2.3.0). Available from: <http://www.openfoam.com/>.
[19] Wang CJ, Wen JX, Lu SX, Guo J. Single-step chemistry model and transport coefficient model for hydrogen combustion. Sci China Tech Sci 2012;55:2163–8.
[20] Bane SPM, Ziegler JL, Shepherd JE. Development of one-step chemistry model for flame and ignition simulation. 2010. GALCIT Report GALTCITFM:2010.002.
[21] Teodorczyk A. Scale effects on hydrogen-air fast deflagrations and detonations in small obstructed channels. J Loss Prev Proc 2008;21:147–53.